Available online at www.sciencedirect.com
ScienceDirect
Trans. Nonferrous Met. Soc. China 33(2023) 2815−2831
Transactions of Nonferrous Metals Society of China
www.tnmsc.cn

Mechanical behavior and failure characteristics of double-layer composite rock-like specimens with two coplanar joints under uniaxial loading

Su LI[1], Hang LIN[1], Qi-bin LIN[1], Yi-xian WANG[2], Yan-lin ZHAO[3], Hui-hua HU[4]

1. School of Resources and Safety Engineering, Central South University, Changsha 410083, China;
2. School of Civil Engineering, Hefei University of Technology, Hefei 230009, China;
3. School of Resource, Environment and Safety Engineering, Hunan University of Science and Technology, Xiangtan 411201, China;
4. Hunan Provincial Transportation Planning Survey and Design Institute Co., Ltd., Changsha 410219, China

Received 14 April 2022; accepted 5 September 2022

Abstract: To study the combined action of joints and bedding plane on crack evolution of flawed layered rock masses, uniaxial compression tests and digital image correlation (DIC) tests were carried out on double-layer composite rock-like specimens with multi-inclination two coplanar joints under different bedding angles. Based on the experimental results, the existence of bedding plane and joints performs a significant effect on characteristics of stress−strain curves and strength parameters. The failure modes are divided into four different types. The existence of bedding plane inhibits the coalescence of cracks in rock bridge area, and the variation of bedding angle affects the crack propagation path and failure mode transition greatly. For specimens with bedding angle of 30° and 45°, the larger the joint angle, the less the influence of bedding plane on failure characteristics. Besides, a new tensile crack type which initiates from the bedding plane and is easier to propagate in the upper layer was observed.

Key words: two coplanar joints; rock-like specimens; crack evolution; uniaxial loading; digital image correlation (DIC) method

1 Introduction

Layered composite rock mass is a common engineering rock mass. The differences in the mechanical properties between adjacent layers, which determine the mechanical behavior of layered composite rock mass will be more complex than that of single lithologic rock mass. Investigating the mechanical properties and crack evolution behavior of composite rock is very meaningful to geotechnical engineering [1,2]. Up till now, many scholars have published research on transversely isotropic rocks through theoretical derivation [3,4], physical experiments [5,6] and numerical simulation [7,8]. ALIABADIAN et al [9,10], VERVOORT et al [11], XU et al [12], TAN et al [13], LI et al [14], and SHANG et al [15] studied the tensile behavior of transversely isotropic rocks by laboratory test or numerical simulation, and the results show that the change of transversely isotropic angle performs a great influence on the peak loading force and the failure mode. YANG et al [16], DOUMA et al [17], and WEN et al [18] studied the loading parameters on crack evolution behavior and mechanical properties of layered rock. XIE et al [19], XU et al [20], YANG et al [21], and WANG et al [22] investigated the influence of layered rock characteristics (layer thickness, layer dip angle, bedding plane properties and difference of adjacent layers) on mechanical characteristics of layered rock by means of numerical simulation and

Corresponding author: Hang LIN, Tel: +86-15388012911, E-mail: linhangabc@126.com
DOI: 10.1016/S1003-6326(23)66300-9

physical experiments. The researches mentioned above systematically and deeply studied the mechanical properties of layered composite rock, but they regarded complete composite rock as the research object and the effect of original flaws on mechanical properties of composite rock were not considered.

In fact, there are a large number of discontinuities in natural rock masses [23−25]. On the one hand, the existence of discontinuities weakens the mechanical parameters of the rock mass [26,27]. On the other hand, under loading conditions, new cracks often occur near the original discontinuities [28,29]. The initiation, propagation and coalescence of cracks will further weaken the mechanical parameters and possibly even lead to the failure of rock mass [30,31]. At present, the study on mechanical parameters and crack evolution of fractured rock mainly concentrated on fractured single lithologic rock [32−35]. About single lithologic rock with two joints, WONG et al [36,37], ZHANG and WONG [38], and YANG [39] systematically studied the influence of joint relative position (coplanar or parallel), joint angle, rock bridge angle and bridge length on the mechanical properties and crack coalescence of fractured rock through different means. In addition, scholars also adopted a variety of advanced technical methods to analyze the mechanical properties of fractured single lithologic rock [40−42].

Up till now, there are relatively few studies involving fractured composite rock masses [43,44]. However, due to the difference of mechanical properties between two adjacent layers, the mechanical behavior of fractured composite rock masses is very different from that of fractured single-lithologic rock masses [45,46]. Considering that fractured composite rock masses are very common in rock engineering, it is of great importance to study the mechanical characteristics of fractured composite rock masses. Therefore, in order to figure out the combined influence of joint angle and bedding angle on the mechanical characteristics and failure process of fractured double-layer composite rock-like specimens under uniaxial loading, a series of axial compression tests were carried out on double-layer composite rock-like specimens with two coplanar joints. The CCD camera was also adopted to track and collect the displacement information of specimens during the whole loading process. Firstly, the influence of bedding angle and joint angle on the mechanical characteristics of specimens is analyzed. Based on the influence degree of prefabricated joints and bedding plane on the final failure of specimens, several classic failure modes are summarized and analyzed based on crack evolution process and stain field nephogram. The effects of joint angle and bedding angle on crack evolution characteristics and transition of failure modes are analyzed and the research results can provide reference for crack evolution of flawed bedded rock slopes.

2 Experimental

2.1 Specimen preparation

Flawed layered composite rock masses are often encountered in geotechnical engineering, as shown in Fig. 1(a). The model of composite rock specimen with two coplanar joints in this experiment is obtained by simplifying the actual engineering rock masses, which is illustrated in

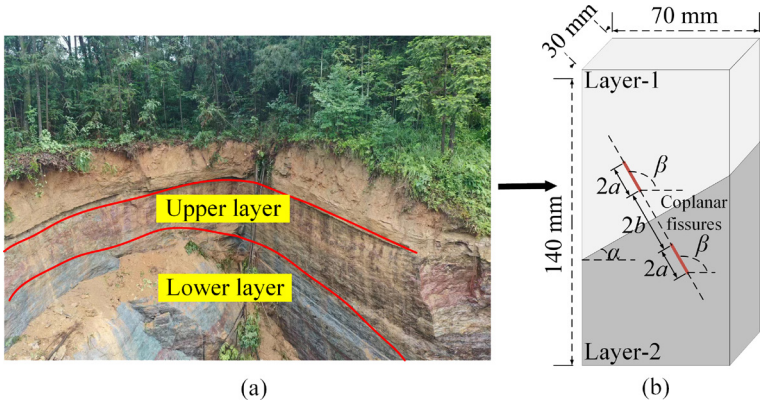

Fig. 1 Typical flawed composite rock mass (a); Model of flawed rock-like specimen with two dissimilar layers (α is bedding angle, β is joint angle (ligament angle), $2a$ represents fissure length, and $2b$ represents ligament length) (b)

Fig. 1(b). According to the suggestion of International Society for Rock Mechanics and Rock Engineering (ISRM) [47], the aspect ratio of specimens is 2.0, and the sizes of specimens are 140 mm (height), 70 mm (width) and 30 mm (thickness). Each specimen is assigned a unique number, S-α-β. In this experiment, four bedding angles are selected, which are 0°, 30°, 45° and 60° respectively. Joint angle ranges from 0° to 150° with 30° as an interval. Furthermore, other joint geometric information remains unchanged, with joint length of 15 mm and rock bridge length of 30 mm.

In this experiment, cement mortar specimens were used to simulate double-layer composite rock masses. The upper layer (Layer-1) was made of white cement mortar mixed with P32.5 white cement, fine sand and water. The lower layer (Layer-2) was made of black cement mortar, which is composed of P42.5 black cement, fine sand and water. The volume ratio of cement (white cement and black cement), fine sand and water is 8:8:5. In Fig. 2(a), several slots were cut at the designated position inside the mold and the mold can be divided into two parts after inserting the thin iron sheets into the slots. The specimen was formed by pouring white cement mortar and black cement mortar into the upper and lower parts of the mold, respectively. Half an hour after pouring, the thin iron sheet was pulled out smoothly.

The coplanar joints were fabricated by inserting mica sheets at designated positions, and the sizes of mica sheets are 15 mm (length) and 0.5 mm (thickness). To ensure accuracy, several transparent acrylic plates recorded with joint geometric information were customized, which are shown in Fig. 2(b). The plates were put on top of the molds and mica sheets were inserted at the openings. After 24 h, specimens were demolded and cured following the standard method for 28 d before the experiment. Specimens with bedding angle of 30° are shown in Fig. 2(c). In addition, to obtain the basic mechanical parameters of intact specimens, a number of standard cylindrical specimens used for uniaxial compression tests and Brazilian splitting tests were made following the recommendation of ISRM [48]. The IDs of intact specimens are I-B, I-W and I-BW, representing intact black cement specimen, intact white cement specimen and Intact double-layer composite specimen. The basic mechanical parameters of intact specimens are listed in Table 1.

2.2 DIC method

The principle of DIC method is to mesh the speckle surface of the specimen and divide it into several subsets. By comparing and analyzing the images of subsets before and after deformation, the coordinate difference of each pixel in the subset can

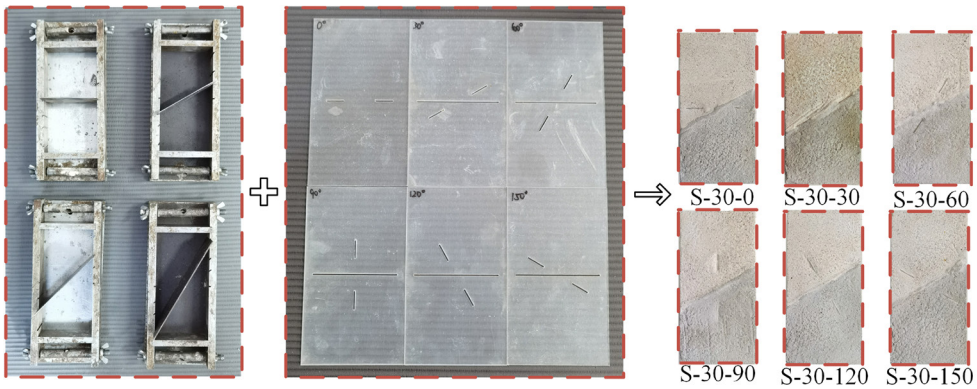

(a) Bedding plane (b) Fissure geometry (c) Specimens (α=30°)

Fig. 2 Preparation of double-layer composite rock-like specimens with two coplanar joints

Table 1 Basic mechanical parameters of intact specimens

Specimen ID	Uniaxial compressive strength/MPa	Uniaxial tensile strength/MPa	Peak strain/10^{-3}	Elastic modulus/GPa
I-B	41.771	5.671	14.806	4.576
I-W	35.295	7.171	14.478	4.330
I-BW	36.501	–	14.343	4.233

be obtained and the displacement of every subset can be then calculated. Using this method, the displacement field can be obtained through calculating the displacement of each sunset, and the strain field can be further calculated by Cauchy equation [49]. To fulfill the requirements of the DIC experiment, specimens should be speckled before the test. Firstly, the specimen was polished and the dust was removed. A layer of white paint was then sprayed on the specimen surface to improve the smoothness and viscosity, which is convenient for speckling. After the primer was dried, black paint was sprayed on the primer evenly and randomly.

2.3 Experimental setup

Figure 3 describes the layout of the experimental setup in this study, which consists of a test system, a data collection system and a DIC system. The test system is an electro-hydraulic servo testing machine, which is composed of loading equipment, servo equipment and control system. Two loading methods, displacement control and force control, are provided. Displacement control mode is adopted in this experiment and the loading rate is 0.01mm/min. Data collection system consists of a computer (collecting force−displacement data from the testing system) and a Canon high-speed camera (synchronously recording crack evolution behavior during loading). The DIC system consists of a charge coupled device camera, two white lights and a computer used for controlling and recording. Before testing, high-speed camera and CCD camera were respectively arranged on the front and back of the specimen and adjusted to ensure the center of the specimen and the camera lens on the same horizontal line. Then, the aperture size and focal length were adjusted to make the speckle image clearly. Finally, the photographic speed was set to15 frames per second.

3 Results

3.1 Complete stress−strain curves

According to the difference of bedding angle, the original data are processed to draw the whole stress−strain curves of double-layer composite specimens with two coplanar joints under uniaxial loading. As shown in Fig. 4, the changes of bedding angle and joint angle have certain effects on the characteristics of stress−strain curves. Although there are some differences in each curve, they all contain four classic stages, which are stage-1 (microcrack compaction stage), stage-2 (elastic deformation stage), stage-3 (microcrack propagation stage) and stage-4 (post-peak stage), as shown in Fig. 4(d). In the early stages of loading, all curves show a concave upward shape, that is, the strain increases greatly and the stress increases little. This is mainly due to the closure of the original cracks in specimens. With an increase in force, the curves enter the elastic deformation stage. In this stage, there is a linear relationship between stress and strain. Before the curve reaches the peak, it is not difficult to find that some curves show stress drop, such as S-30-150 and S-45-120, which is mainly caused by the appearance of macroscopic cracks in the pre-peak stage. The characteristics of stress−strain curves in the post-peak stage are also different. Some curves show a large stress drop rapidly after entering the post-peak stage, and other curves have to go through several small stress drops. The effect of bedding angle on the characteristics of

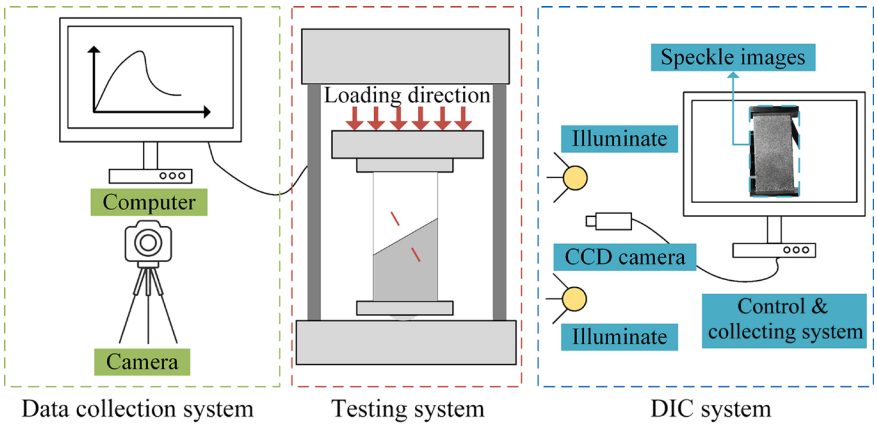

Fig. 3 Sketch of experiment setup

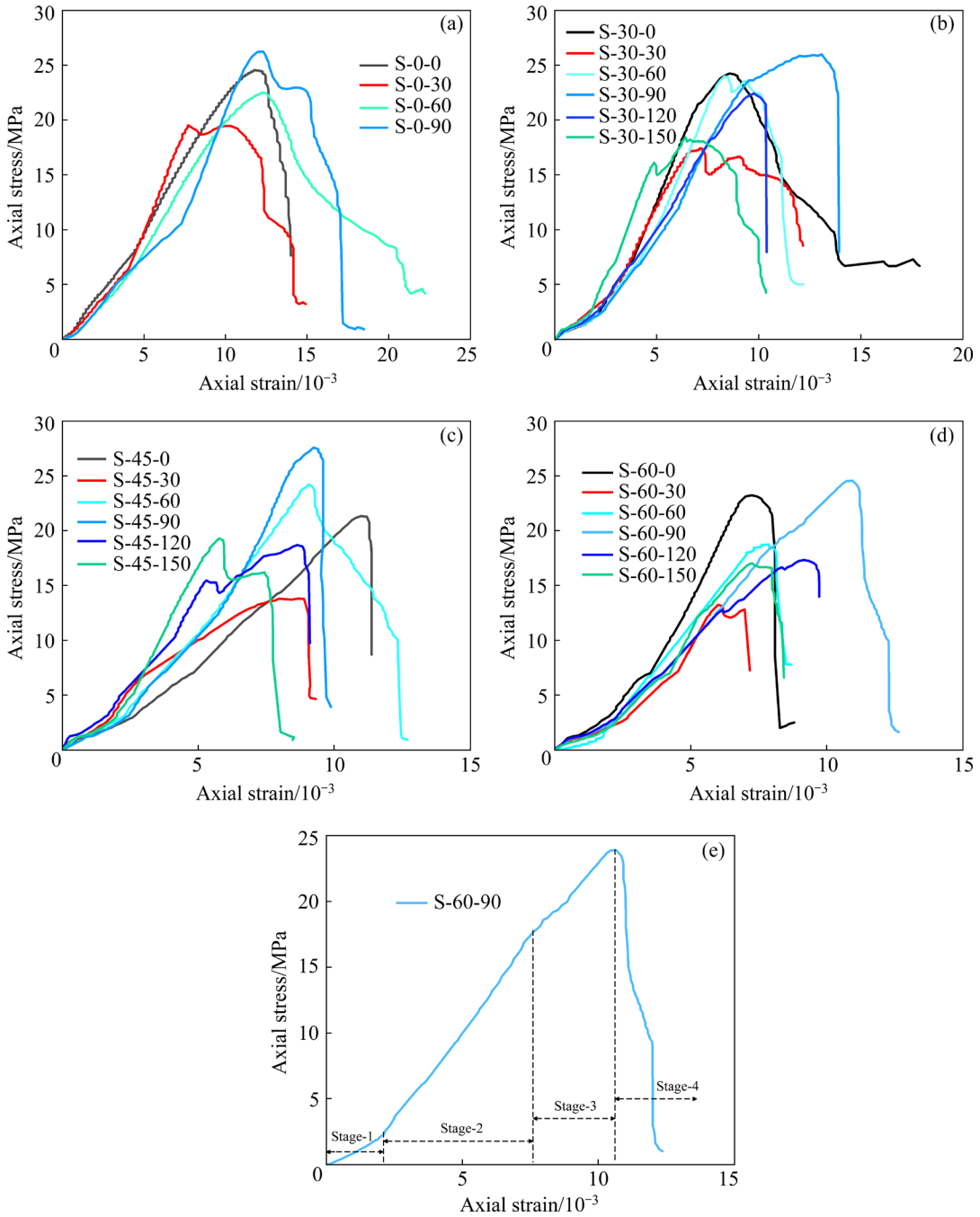

Fig. 4 Complete stress−strain curves of double-layer composite rock-like specimens with two coplanar joints: (a) α=0°; (b) α=30°; (c) α=45°; (d, e) α=60°

the stress−strain curve is mainly reflected in the post-peak stage. With increased bedding angle, the proportion of a large stress drop appearing in the post-peak stage is also rising.

3.2 Mechanical parameters

To better understand the influence of bedding angle and joint angle on the strength parameters of flawed double-layer composite specimens, the experimental data are processed to obtain the basic mechanical parameters of specimens, including peak stress and peak strain. Mechanical parameter curves of flawed double-layer composite specimens varying with joint angle are shown in Fig. 5. Compared with the mechanical parameters of the intact specimen, it is obvious that the existence of joints and inclined bedding plane weakens the mechanical parameters of the specimen.

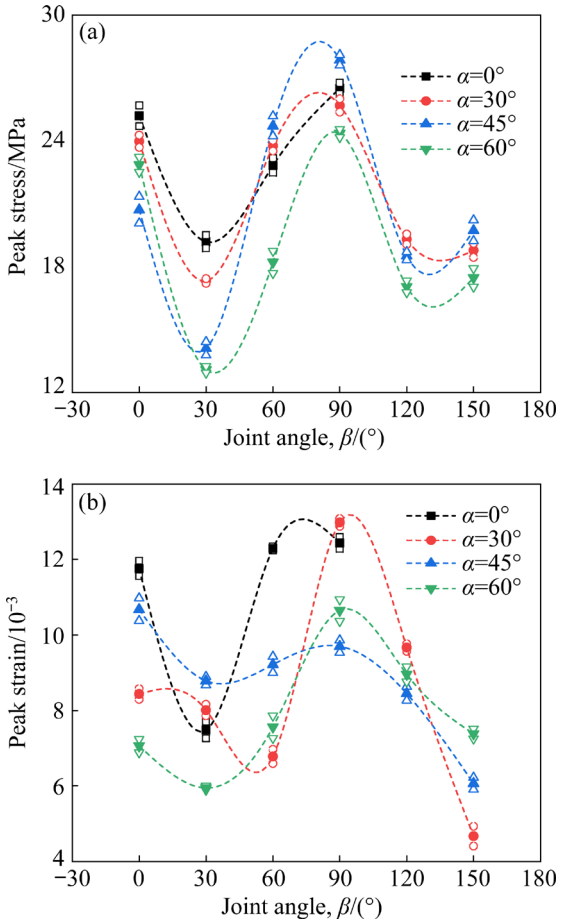

Fig. 5 Mechanical parameter curves of double-layer composite rock-like specimens with two coplanar joints under uniaxial loading: (a) Peak strength versus joint angle; (b) Peak strain versus joint angle

In Fig. 5(a), it can be seen that the variation in joint angle appears to have a great influence on the peak strength of specimens, and the influence law is obvious. All curves show a "W" shape. No matter how the bedding angle changes, each curve reaches its minimum when the joint angle is 30° and its maximum when the joint angle equals 90°. In addition, though the peak strength curve is not "W" shape when the bedding angle is 0°, the variation trend in the interval of [0,90] shows a good consistency with other curves. When bedding angle is 60° and joint angle is 30°, the peak strength of flawed double-layer composite specimen reaches a minimum of 13.086 MPa, which is 64.15% lower than that of the intact double-layer composite specimen. When bedding angle is 45° and joint angle is 90°, the peak strength of flawed double-layer composite specimen reaches a maximum of 27.851 MPa, which is 23.70% lower than that of the intact double-layer composite specimen.

In Fig. 5(b), all peak strain curves show a trend of decreasing first, then increasing and finally decreasing with the variation of joint angle (the variation law of curves with bedding angle of 0° is consistent with that of other curves from 0° to 90°). Except that when the bedding angle is 60°, the curve reaches the minimum when joint angle is equal to 30°, other curves reach the minimum when joint angle is 150° and the maximum when the joint angle equals 90°. The peak strain of the intact double-layer composite specimen is 14.343×10^{-3}. By comparison, the peak strain of flawed specimens decreases in various degrees. When the bedding angle is 30° and the joint angle is 150°, the peak strain of flawed double-layer composite specimen reaches the minimum of 4.673×10^{-3}, which is 67.42% lower than that of the intact double-layer composite specimen. When the bedding angle is 30° and the joint angle is 90°, the peak strain of flawed double-layer composite specimen reaches the minimum of 12.981×10^{-3}, which is 9.50% lower than that of the intact double-layer composite specimen.

4 Analysis and discussion

High-speed camera and CCD camera were adopted to record the successive crack evolution behavior and speckle images with displacement information respectively. Speckle images were processed by GOM Correlate software to observe the strain field evolution during the whole loading process. Based on crack propagation behavior and principal strain field, crack evolution processes of double-layer composite specimens with two coplanar joints were analyzed. Besides, the influence of joint angle and bedding angle on failure characteristics of flawed specimens was also studied.

4.1 Classic failure modes

Based on the analysis of crack evolution process and strain field nephogram, failure modes of double-layer composite specimens with two coplanar joints can be divided into four types depending on the contribution of joints and bedding plane to the ultimate failure of specimens. These four failure modes are single-joint dominant failure mode, double-joint dominant failure mode, mixed

mode, and bedding plane dominant failure mode, as shown in Figs. 6−9. All stages (a) and (a′) in Fig. 6 to Fig. 9 are taken as reference pictures.

4.1.1 Single-joint dominant failure mode

Figure 6 shows the crack propagation process and the principal strain field corresponding to single-joint dominant failure mode. The ultimate failure of specimen is caused by the initiation, propagation and coalescence of cracks initiated at joint tips in the weak layer (stages (e) and (e′)). With the axial loading applied to the end of the specimen, blue strain concentration areas first appear at the tips of pre-existing joints. The color of strain concentration area at the lower joint tips is light and almost unchanged, which means that there are no macro-cracks at the tips of the joint in the lower layer during the whole loading process. The strain concentration areas in the upper part of the specimen initiate from the tips of the joints and are approximately parallel to the loading direction. As loading continues, a coplanar strain concentration zone appears at the outer tip of the upper joint and the initial strain concentration zone stops changing, indicating that a coplanar shear crack occurs at the upper joint tip. Meanwhile, a non-coplanar strain concentration zone is shown in the upper part of the specimen, and the strain concentration zone located at the inner tip of the upper joint also expands with the increase of axial force. Tensile wing crack can also be observed at the inner tip of the upper joint and penetrates the bedding plane. The specimen fails when the coplanar strain concentration zone coalesces with the strain concentrations zone near the joint tip.

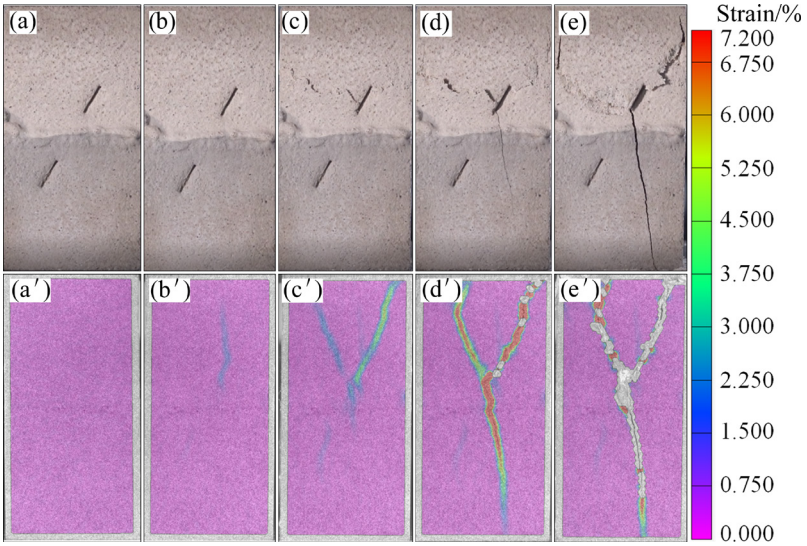

Fig. 6 Failure process and principal strain field corresponding to single-joint dominant failure mode (S-0-60)

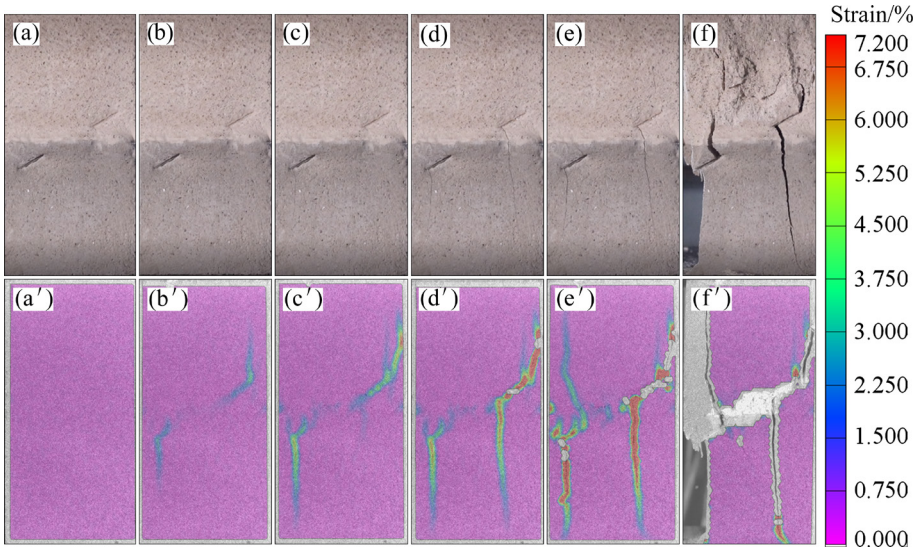

Fig. 7 Failure process and principal strain field corresponding to double-joint dominant failure mode (S-0-30)

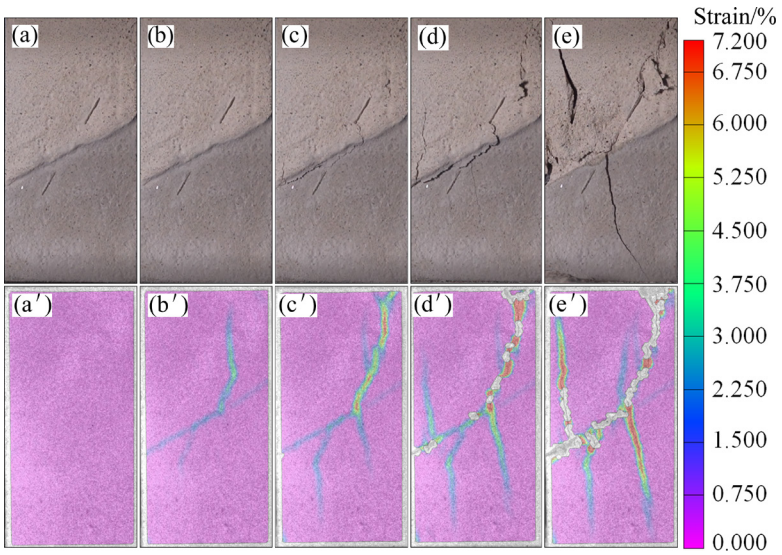

Fig. 8 Failure process and principal strain field corresponding to mixed failure mode (S-30-60)

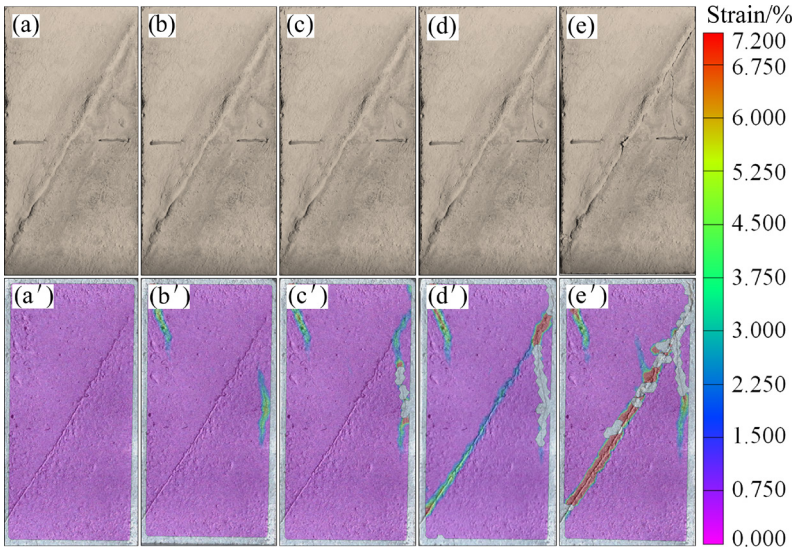

Fig. 9 Failure process and principal strain field corresponding to bedding plane dominant failure mode (S-60-0)

4.1.2 Double-joint dominant failure mode

Figure 7 represents the crack evolution behavior and the principal strain field nephogram corresponding to double-joint dominant failure mode. From the final failure characteristic and the last stage of strain field, it can be found that the failure of the specimen is caused by the successive crack evolution behavior initiated from the tips of two prefabricated joints (stages (f) and (f′)). When axial force is applied to the specimen, strain concentration zones initiate at the tips of joints and are roughly parallel to the vertical direction, as shown in Fig. 7(b′). At this time, strain concentration is low, and no macro-cracks are observed on the specimen surface. With the increase of load, strain concentration zone at the outer tip of the joint in the lower layer expands along the loading direction, while strain concentration zone at the inner tip stops changing (stage (c′)). A non-coplanar strain concentration zone appears at the right side of the upper layer, which extends along the inclined direction. When the non-coplanar strain concentration zone coalesces with the upper joint, the stain concentration zone at the inner tip of the upper joint propagates suddenly along the axial direction, as shown in Figs. 7(c′) and (d′). Compared with the corresponding crack evolution stage, a tensile wing crack initiates from the inner tip of the upper joint and propagates along the axial direction. In stage (e′), a strain concentration zone

appears at the inner tip of the lower joint and propagates upward. Similarly, a tensile wing crack is observed at the inner tip of the lower joint in stage (e). All strain concentration bands extend to the boundary of the specimen with further increase of axial load, finally resulting in the failure of the specimen, as shown in stage (f′). It is worth noting that the generation of strain concentration zone in rock bridge area does not mean that there are macro-cracks in the rock bridge area, but they are caused by the extrusion in rock bridge area (stage (f′)).

4.1.3 Mixed failure mode

Figure 8 represents the crack evolution behavior and strain field nephogram corresponding to mixed failure mode. Specifically, the failure of the specimen is caused by cracks initiated from joint tips and the shear crack on the bedding plane (stages (e) and (e′)). It can be clearly seen that strain concentration bands initiate at the tips of joint in the upper layer, as shown in Fig. 8(b′). However, the strain concentration band at the outer tip stops expanding. A coplanar strain concentration band and a non-coplanar strain concentration band respectively appear at the outer tip of the upper joint and the right side of the upper layer and continue to propagate. Simultaneously, there are strain concentration bands appear at the bedding plane and the lower joint tips, but the strain is small, as shown in Fig. 8(c′). In stage (d′) of strain field, the strain concentration band at the inner tip of the upper joint propagates and penetrates the bedding plane. The strain concentration zone located on the bedding plane expands upward. Additionally, the strain concentration bands at the tips of the lower joint continue to expand, and tensile wing cracks can be observed at the tips of the lower joint in stage (d) of crack evolution process. As load continues to increase, the specimen loses its bearing capacity when the strain concentration band on bedding plane turns red (stage (e′)).

4.1.4 Bedding plane dominant failure mode

Figure 9 shows the crack evolution process and strain field corresponding to bedding plane dominant failure mode. This mode does not mean that cracks only initiate on the bedding plane, but that the bedding plane dominates the ultimate failure of the specimen (stages (e) and (e′)). As shown in Fig. 9, strain concentration bands first initiate at the tips of the lower joint and propagate along the axial direction (stage (b′)). The strain concentration band which propagates upward does not penetrate the bedding plane after reaching it, but extends along the bedding plane, as shown in stage (c′). The specimen fails when the color of the inclined strain concentration band on the bedding plane changes from blue to red (stage (e′)). As clearly shown in crack evolution process, the crack first initiates near the outer tip of the right joint. The tensile crack which propagates upward will expand along the bedding plane after reaching it, as shown in stage (d). However, the specimen does not completely lose its bearing capacity. The specimen is destroyed when the bedding plane slides under the action of shear force, as shown in stage (e).

4.2 Crack types and characteristics

Many scholars have conducted in-depth systematic research on crack initiation, propagation and coalescence of flawed rock masses under uniaxial loading, and defined various crack types. These results can help us to analyze and understand crack evolution behavior in this study. There are only eight crack types observed in this work compared with crack types summarized by other scholars, as shown in Fig. 10. These eight types are tensile crack-1 (crack initiates at the joint tip), tensile crack-2 (crack initiates from the middle part

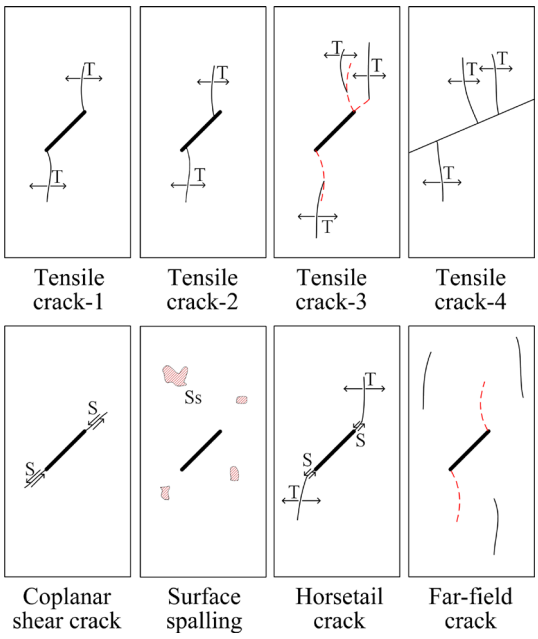

Fig. 10 Crack types of double-layer composite rock-like specimens with two coplanar joints observed in this study (T: Tensile crack; S: Shear crack; Ss: Surface spalling)

of joint), tensile crack-3 (out-of-plane tensile crack), tensile crack-4, coplanar shear crack, horsetail crack (a crack combined by a coplanar shear crack and a out-of-plane tensile crack), far-field crack and surface spalling. The difference between far-field crack and out-of-plane tensile crack is that far-field crack will not coalesce with cracks initiated from the prefabricated joint. In addition, a new tensile crack type is observed, which initiates from the bedding plane and propagates toward one layer of the specimen.

Since some crack paths are thin and the crack propagation speed is very fast when the final failure happens, it is really difficult to accurately recognize the crack path by naked eyes. Besides, the crack initiation usually shows no obvious characteristics and some cracks almost initiate simultaneously, making it hard to distinguish crack initiation sequence even with the help of high-speed camera recording. Hence, scholars typically adopt several auxiliary techniques to record and qualitatively analyze crack evolution behavior. High-speed camera can record the crack propagation path of the specimen. Propagation direction and appearance time of high strain concentration band in strain field nephogram can help to distinguish the crack types and the sequence of crack initiation. As shown in Fig. 11, crack evolution diagrams of flawed specimens under uniaxial loading are drawn based on the camera recordings and the evolution of strain field nephograms. In Fig. 11, each crack has a corresponding number, which is composed of a letter and a number. Letter represents crack type and number represents the order of crack initiation. In addition, the black arrow represents the propagation direction of the crack after reaching the bedding plane, the red arrow represents the sliding direction of the upper layer, and the red shadow part represents surface spalling.

In Fig. 11, the crack propagation path of the specimen under uniaxial loading is relatively curved, mainly due to the anisotropy of the specimen. As shown in Fig. 11, the number of cracks in the upper layer is usually more than that in the lower layer. For most double-layer composite specimens with two coplanar joints, tensile crack-1 is usually the first initiated crack. For S-0-0, the first crack initiates in the upper layer of the specimen, which is almost similar to the crack initiation mode of the complete specimen under uniaxial loading. Regardless of the joint angle, shear cracks initiate from the tips of pre-existing joints and propagate. From Fig. 11, when bedding angle is 0°, the tensile crack which initiates from the upper joint tip can penetrate the bedding plane directly. For specimens with bedding angle of 30° or 45°, the crack which initiates from the upper tip can only penetrate the bedding plane after extending on the bedding plane for a distance and the distance is proportional to the bedding angle. When the bedding angle equals 60°, the crack will propagate along the bedding plane to the boundary of the specimen rather than penetrating into the adjacent layer. In addition, the cracks initiated from the upper joint usually propagate downward along the bedding plane when they reach the bedding plane, and the cracks initiated from the lower joint usually propagate upward along the bedding plane when they reach the bedding plane. Tensile crack-4 only occurs in specimens when bedding angle is 30°,45° or 60° and suck cracks are more likely to initiate in the upper layer. Else, it is not difficult to find from Fig. 11 that the existence of bedding plane inhibits the coalescence of cracks in rock bridge area. There is usually no direct crack coalescence occurring in rock bridge area. The variation of bedding angle shows an inconspicuous effect on the coalescence of cracks initiated from the inner tips of joints.

4.3 Discussion

Due to the difference of mechanical properties between the upper and lower layers of fractured composite specimens. The crack initiation time and propagation speed are different. Hence, the failure characteristics of single-lithologic specimens with two coplanar joints cannot comprehensively help us to understand the failure characteristics of composite specimens with two coplanar joints. According to the research results of WONG [37] and YANG [39], the failure mode of single-lithologic specimens with two coplanar joints can be considered as double-joint dominant failure modes. Specifically, the failure is dominated by cracks initiated at tips of prefabricated joints, and the cracks initiate almost at the same time from joint tips. Besides, cracks will coalesce in the rock bridge area, and there are two coalescence type. Based on Fig. 11 and Table 2, it is easy to find that compared with single-lithologic specimens with two

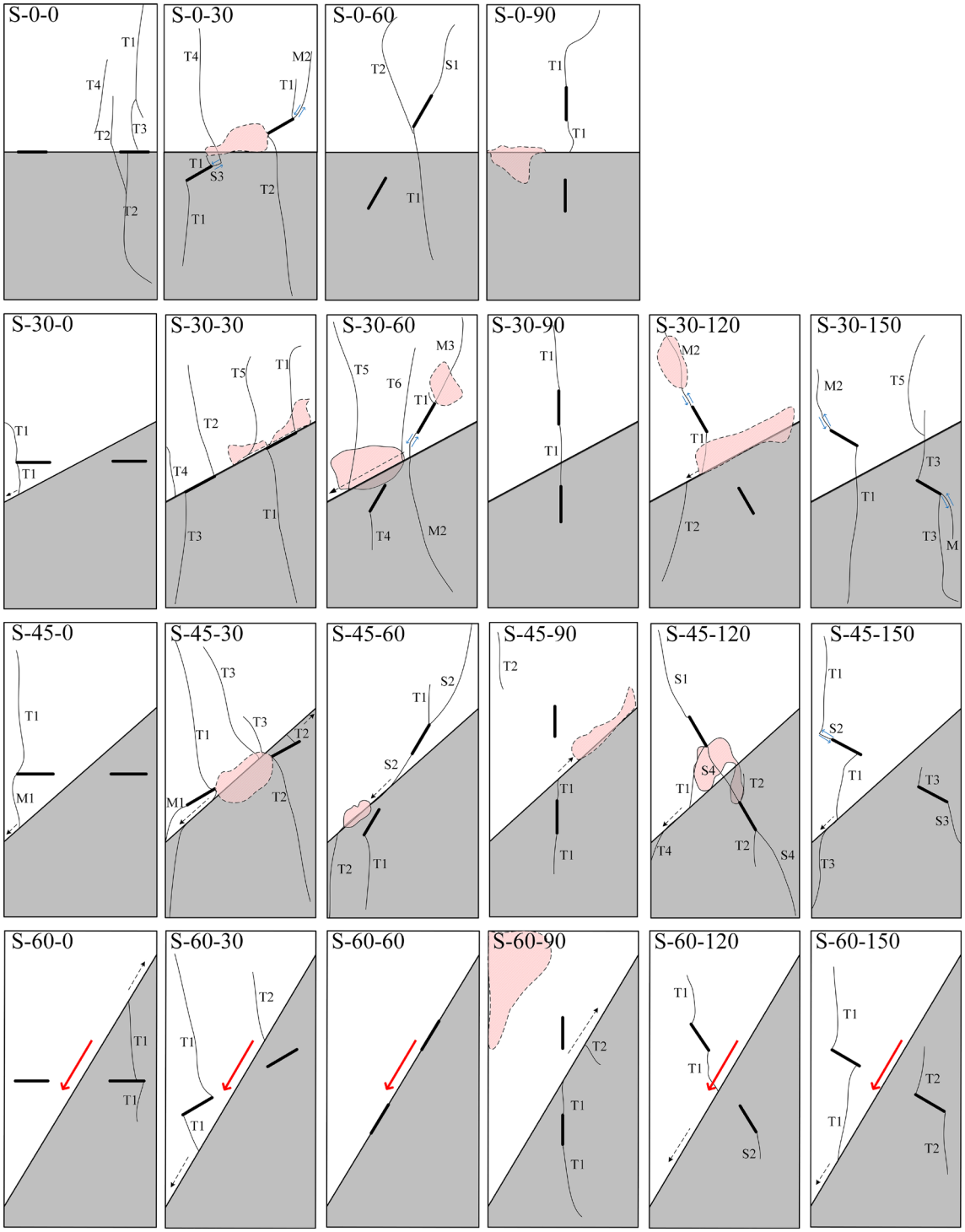

Fig. 11 Sketch of final failure characteristics of double-layer composite rock-like specimens with two coplanar joints based on high-speed camera and DIC results (The horsetail crack in Fig. 10 is named mixed crack (M))

coplanar joints, the failure mode of double- layer composite specimens with two coplanar joints is more complex. No matter how the bedding angle and joint angle vary, there will be no coalescence in the rock bridge area.

When the bedding angle equals 0°, the failure modes of flawed double-layer composite specimens can be divided into single-joint dominant failure mode and double-joint dominant failure mode. The failure of specimens is only caused by the cracks initiated from the joint tips, which is similar to the findings of HU et al [43]. Additionally, for specimens with single-joint dominant failure mode, the cracks only initiate from the joint tips in the

Table 2 Failure modes of double-layer composite rock-like specimens with two coplanar joints

β/(°)	α=0°	α=30°	α=45°	α=60°
0	Single-joint dominant mode	Single-joint dominant failure	Single-joint dominant failure	Bedding plane dominant mode
30	Double-joint dominant mode	Mixed mode	Mixed mode	Bedding plane dominant mode
60	Single-joint dominant mode	Mixed mode	Mixed mode	Bedding plane dominant mode
90	Single-joint dominant mode	Double-joint dominant mode	Mixed mode	Mixed mode
120		Single-joint dominant mode	Mixed mode	Bedding plane dominant mode
150		Double-joint dominant mode	Single-joint dominant mode	Bedding plane dominant mode

upper layer. When bedding angle is 30° and 45°, failure modes of specimens are relatively complex. For specimens with joint angle of 0°, the failure mode is single-joint dominated mode. Cracks initiate from the left joint tips and then propagate with the increasing load. There are no macro-cracks initiated from the right joint tips. For specimens with joint angle of 30° and 60°, the failure mode is mixed mode. Cracks initiate not only from the joint tips, but also from the bedding plane. Although the failure characteristics for specimens with joint angle of 150° are different, it can be seen that cracks initiate from the joint tips and propagate to the boundary of specimens. There are no shear cracks generated on the bedding plane, and the failure is dominated by the prefabricated joints. When bedding angle is 60°, the specimen fails when the upper layer slides along the bedding plane. For S-60-60, only shear cracks appear on the bedding plane. For other specimens with bedding angle of 60°, cracks initiate from the joint tips. However, instead of penetrating into the adjacent layer, the cracks will propagate along the bedding plane when they propagate to the bedding plane.

To better understand the influence of bedding angle and joint angle on the failure characteristics of specimens, two groups of representative specimens' ultimate failure images and corresponding strain field nephograms are selected for comparative analysis, as shown in Figs. 12 and 13. Figure 12 shows a comparison of the ultimate failure modes of flawed double-layer composite specimens with fixed bedding angle (α=30°) and different joint angles (β=0°, 30°, 60°, 90°, 120° and 150°). With the increase of joint angle, the failure characteristics of specimens with bedding angle of 30° are quite different. When joint angles are 30° and 60°, cracks initiate from joint tips and bedding plane dominate the failure of specimens. An inclined stripe high strain concentration band can also be observed on the bedding plane from the strain field nephogram. However, when the joint angle is from 90° to 150°, the effect of bedding plane on the failure of specimens is weakened. The failure is only affected by the cracks initiating from the joint tips, which can be verified by the fact that there is no high strain concentration band appears on the bedding plane. Figure 13 shows a comparison of the final failure modes of flawed double-layer composite specimens with fixed joint angle (β=60°), and varied bedding angle (α=0°, 30°, 45° and 60°). It can be found that with the increase of bedding angle, the failure mode of the specimen changes from single-joint dominant failure mode (S-0-60) to mixed failure mode (S-30-60 and S-45-60), and then to bedding plane dominant failure mode (S-60-60). The factor that dominates the failure changes from prefabricated joints to the bedding plane with the increase of bedding angle.

The failure of engineering rock masses is typically caused by the propagation and coalescence of cracks initiated from the original flaws, and the crack propagation behavior is greatly affected by the flaw geometries. The experimental results in this study can predict the crack evolution process in two adjacent layers with inclined flaws of bedded rock slopes, as illustrated in Fig. 14.

Figure 14(a) presents the flawed layered slope model with horizontal bedding planes. The cracks initiate around the original flaws and propagate

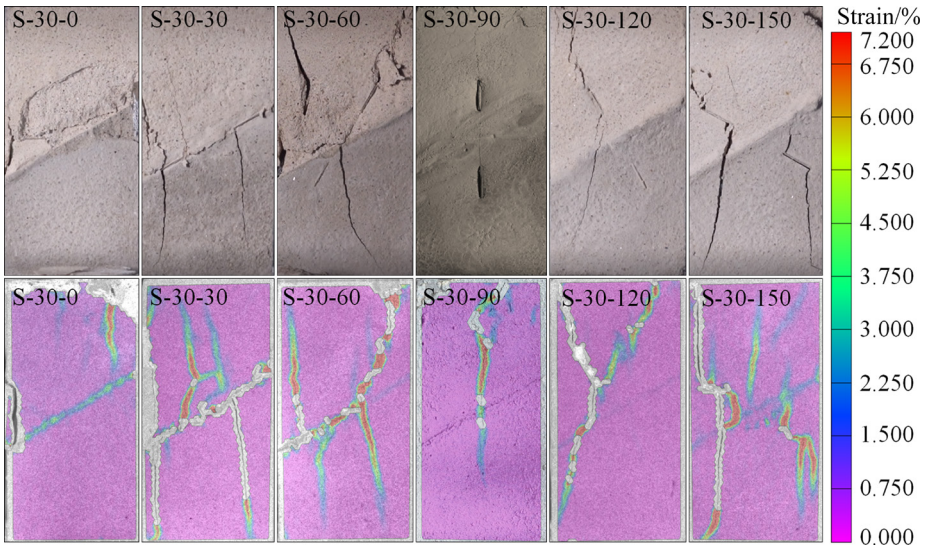

Fig. 12 Final failure modes and corresponding strain field of flawed double-layer composite rock-like specimens with fixed bedding angle and different joint angles

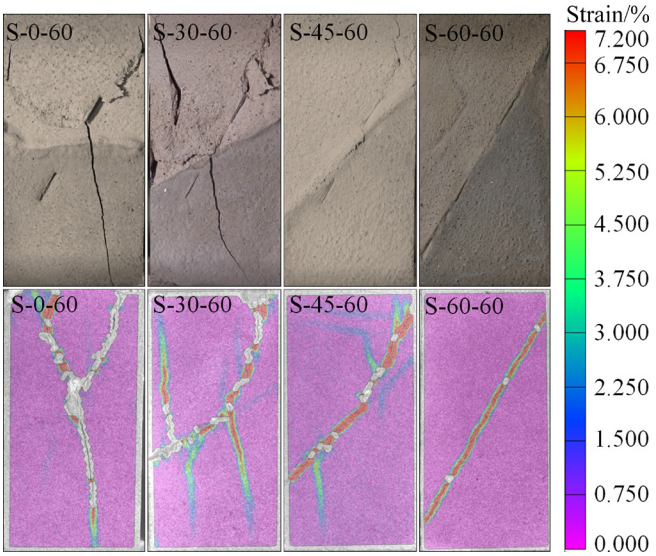

Fig. 13 Final failure modes and corresponding strain field of flawed double-layer composite rock-like specimens with fixed joint angle and different bedding angles

upward and downward. The crack will penetrate the bedding plane directly to the adjacent layer, and no shear sliding appears on the bedding plane. Figures 14(b) and (c) show the flawed layered slope model with pro-dip bedding planes, with the orientation of bedding planes being 30° and 45° respectively. The crack which initiates from original flaw will transform into shear sliding cracks after reaching the bedding plane. The shear sliding crack will transform into tensile crack after propagating a certain distance along the bedding plane. It should be noted that when the bedding angle is 30° and the flaw angle is 150°, the crack will penetrate the bedding plane directly; when the bedding angle is 45°, the crack will turn into shear sliding crack when reaching the bedding plane, no matter how the flaw angle varies. Figure 14(d) illustrates the flawed layered slope model with pro-dip bedding planes, and the bedding angle is 60°. Compared with the middle two cases, the tensile crack initiated from the original flaw will transform into shear sliding crack after extending to the bedding plane, but the shear sliding crack will not penetrate to the adjacent layer and the number of cracks generated in each layer is also less. The shear sliding crack on the bedding plane dominates

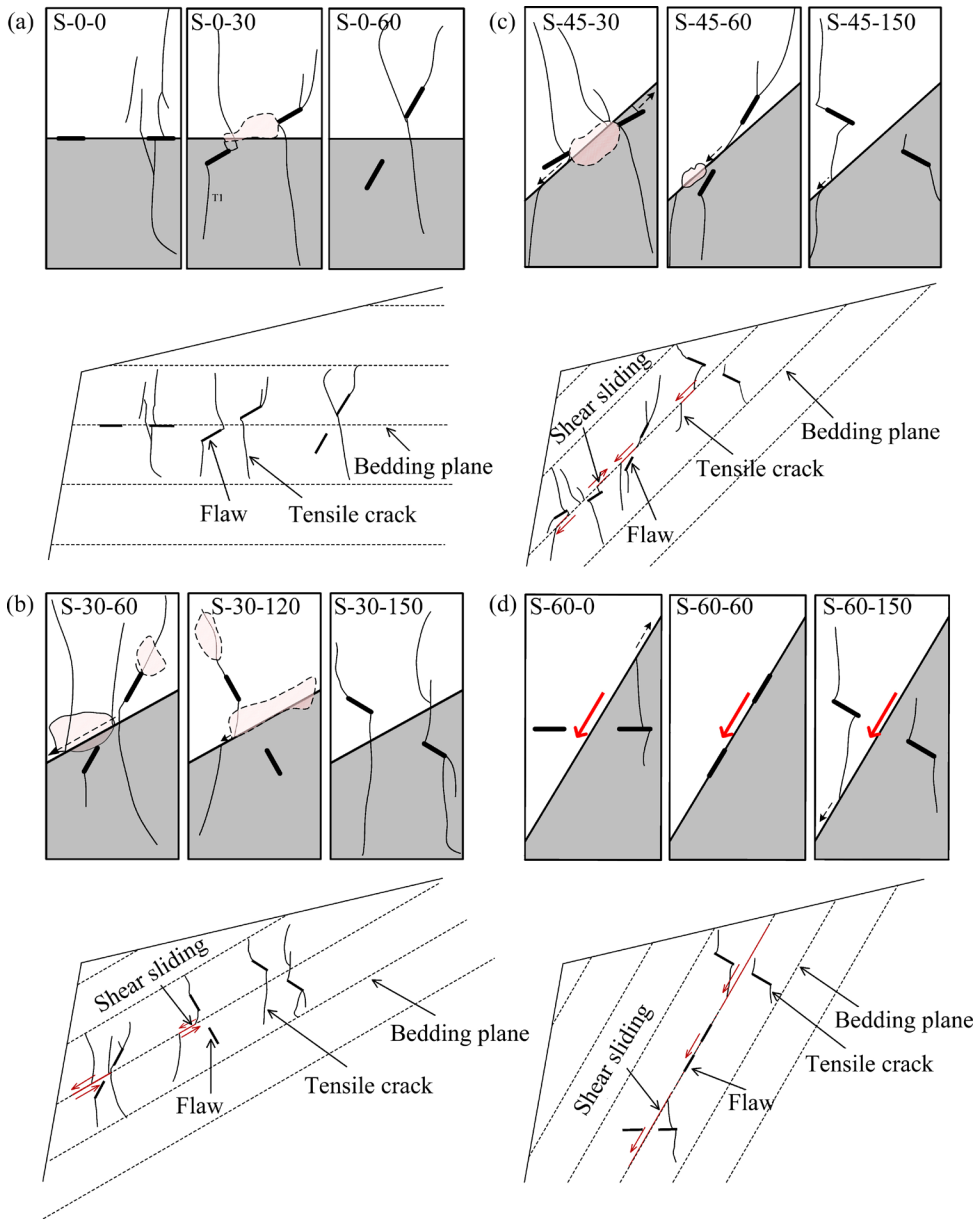

Fig. 14 Crack evolution behavior in two adjacent layers with flaws of layered rock slopes: (a) 0°; (b) 30°; (c) 45°; (d) 60°

the crack evolution process.

5 Conclusions

(1) The variation of joint angle affects the mechanical parameters of specimens greatly. The peak strength of fractured specimens ranges from 13.241 to 27.601 MPa, which is 24.38% to 63.72% lower than that of intact specimen. The peak strain of fractured specimens is reduced by 8.78% to 58.78% compared with intact composite specimen. The bedding angle has a great influence on the post-peak characteristics of stress−strain curves. With the increase of bedding angle, the post-peak stage of stress-strain curves is easy to perform a significant stress drop.

(2) The failure modes are divided into four types: single-joint dominant failure mode, double-joint dominant failure mode, mixed failure mode and bedding plane dominant failure mode. The greater the bedding angle, the more significant influence of bedding plane on failure mode. For specimens with middle bedding angle (α=30° and 45°), with the increase of joint angle, the failure mode changes from mixed failure mode to joint dominant failure mode.

(3) The bigger the bedding angle, the lower the possibility of cracks penetrating into the adjacent layer. For specimens with high bedding angle (α=60°), cracks cannot penetrate into the adjacent layer. In addition, the existence of bedding plane inhibits the coalescence of cracks in rock bridge area. A new crack type is observed which usually initiates on the bedding plane when the final failure happens and is more likely to generate in the upper layer.

Acknowledgments

This work is supported by the National Natural Science Foundation of China (No. 51774322), Hunan Provincial Key Research and Development Program, China (No. 2022SK2082), Hunan Provincial Natural Science Foundation of China (No. 2018JJ2500), Fundamental Research Funds for the Central Universities of Central South University, China (No. 2021zzts0275), Western Transportation Construction Technology Project, China (No. 200631879846), and Science and Technology Progress and Innovation Plan of Hunan Provincial Department of Transportation, China (No. 2010003).

References

[1] LEI Da-xing, LIN Hang, WANG Yi-xian. Damage characteristics of shear strength of joints under freeze–thaw cycles [J]. Archive of Applied Mechanics, 2022, 92: 1615−1631.

[2] FAN Xiang, YU Hao, DENG Zhi-ying, HE Zhong-ming, ZHAO Yan-lin. Cracking and deformation of cuboidal sandstone with a single nonpenetrating flaw under uniaxial compression [J]. Theoretical and Applied Fracture Mechanics, 2022, 119: 103284.

[3] ALNEASAN M, BEHNIA M, BAGHERPOUR R. Analytical investigations of interface crack growth between two dissimilar rock layers under compression and tension [J]. Engineering Geology, 2019, 259: 105188.

[4] XU Guo-wen, HE Chuan, YAN Jian, MA Gao-yu. A new transversely isotropic nonlinear creep model for layered phyllite and its application [J]. Bulletin of Engineering Geology and the Environment, 2019, 78: 5387−5408.

[5] CAO Ri-hong, YAO Ru-bing, HU Tao, WANG Chang-song, LI Kai-hui, MENG Jing-jing. Failure and mechanical behavior of transversely isotropic rock under compression-shear tests: Laboratory testing and numerical simulation [J]. Engineering Fracture Mechanics, 2021, 241: 107389.

[6] LIN Hang, SUN Peng-hui, CHEN Yi-fan, ZHU You-yan, FAN Xiang, ZHAO Yan-lin. Analytical and experimental analysis of the shear strength of bolted saw-tooth joints [J]. European Journal of Environmental and Civil Engineering, 2022, 26: 1639−1653.

[7] PARK B, MIN K B. Bonded-particle discrete element modeling of mechanical behavior of transversely isotropic rock [J]. International Journal of Rock Mechanics and Mining Sciences, 2015, 76: 243−255.

[8] WANG S Y, SLOAN S W, TANG C A, ZHU W C. Numerical simulation of the failure mechanism of circular tunnels in transversely isotropic rock masses [J]. Tunnelling and Underground Space Technology, 2012, 32: 231−244.

[9] ALIABADIAN Z, ZHAO G F, RUSSELL A R. Crack development in transversely isotropic sandstone discs subjected to Brazilian tests observed using digital image correlation [J]. International Journal of Rock Mechanics and Mining Sciences, 2019, 119: 211−221.

[10] ALIABADIAN Z, ZHAO G F, RUSSELL A R. Failure, crack initiation and the tensile strength of transversely isotropic rock using the Brazilian test [J]. International Journal of Rock Mechanics and Mining Sciences, 2019, 122: 104073.

[11] VERVOORT A, MIN K B, KONIETZKY H, CHO J W, DEBECKER B, DINH Q D, FRÜHWIRT T, TAVALLALI A. Failure of transversely isotropic rock under Brazilian test conditions [J]. International Journal of Rock Mechanics and Mining Sciences, 2014, 70: 343−352.

[12] XU Guo-wen, HE Chuan, CHEN Zi-quan, WU Di. Effects of the micro-structure and micro-parameters on the mechanical behaviour of transversely isotropic rock in Brazilian tests [J]. Acta Geotechnica, 2018, 13: 887−910.

[13] TAN Xin, KONIETZKY H, FRÜHWIRT T, DAN D. Brazilian tests on transversely isotropic rocks: Laboratory testing and numerical simulations [J]. Rock Mechanics and Rock Engineering, 2015, 48: 1341−1351.

[14] LI Kai-hui, YIN Zhen-yu, CHENG Yung-ming, CAO Ping, MENG Jing-jing. Three-dimensional discrete element simulation of indirect tensile behaviour of a transversely isotropic rock [J]. International Journal for Numerical and Analytical Methods in Geomechanics 2020, 44: 1812−1832.

[15] SHANG J, DUAN K, GUI Y, HANDLEY K, ZHAO Z. Numerical investigation of the direct tensile behaviour of laminated and transversely isotropic rocks containing incipient bedding planes with different strengths [J]. Computers and Geotechnics, 2018, 104: 373−388.

[16] YANG Sheng-qi, YIN Peng-fei, HUANG Yan-hua, CHENG Jian-long. Strength, deformability and X-ray micro-CT observations of transversely isotropic composite rock under different confining pressures [J]. Engineering Fracture Mechanics, 2019, 214: 1−20.

[17] DOUMA L A N R, REGELINK J A, BERTOTTI G, BOERSMA Q D, BARNHOORN A. The mechanical contrast between layers controls fracture containment in layered rocks [J]. Journal of Structural Geology, 2019, 127: 103856.

[18] WEN Sen, ZHANG Chun-shun, CHANG Yu-lin, HU Ping. Dynamic compression characteristics of layered rock mass of significant strength changes in adjacent layers [J]. Journal of Rock Mechanics and Geotechnical Engineering, 2020, 12: 353−365.

[19] XIE Li-quan, JIN Peng, SU Tsung-Chow, LI Xiao-bo, LIANG Ze-long. Numerical simulation of uniaxial compression tests on layered rock specimens using the discrete element method [J]. Computational Particle

Mechanics, 2020, 7: 753−762.
[20] XU Guo-wen, HE Chuan, CHEN Zi-quan, YANG Qing-hao. Transversely isotropic creep behavior of phyllite and its influence on the long-term safety of the secondary lining of tunnels [J]. Engineering Geology, 2020, 278: 105834.
[21] YANG Xu-xu, JING Hong-wen, QIAO Wei-guo. Numerical investigation of the failure mechanism of transversely isotropic rocks with a particle flow modeling method [J]. Processes, 2018, 6: 171.
[22] WANG Ding-jian, TANG Hui-ming, ELSWORTH D, WANG Chao-yi. Fracture evolution in artificial bedded rocks containing a structural flaw under uniaxial compression [J]. Engineering Geology, 2019, 250: 130−141.
[23] LIU Bo, LIN Hang, CHEN Yi-fan. Deformation characteristics of bolted rock joints under compression-shear load [J]. Applied Sciences, 2022, 12: 5226.
[24] FAN Xiang, YANG Zhi-jun, LI Kai-hui. Effects of the lining structure on mechanical and fracturing behaviors of four-arc shaped tunnels in a jointed rock mass under uniaxial compression [J]. Theoretical and Applied Fracture Mechanics, 2021, 112: 102887.
[25] XIE Shi-jie, LIN Hang, CHEN Yi-fan, WANG Yi-xian. A new nonlinear empirical strength criterion for rocks under conventional triaxial compression [J]. Journal of Central South University, 2021, 28: 1448−1458.
[26] ZHAO Yan-lin, ZHANG Lian-yang, WANG Wei-jun, WAN Wen, MA Wen-hao. Separation of elastoviscoplastic strains of rock and a nonlinear creep model [J]. International Journal of Geomechanics, 2018, 18: 04017129.
[27] ZHAO Yan-lin, ZHANG Lian-yang, WANG Wei-jun, LIU Qiang, TANG Li-ming, CHENG Guo-ming. Experimental study on shear behavior and a revised shear strength model for infilled rock joints [J]. International Journal of Geomechanics, 2020, 20: 04020141.
[28] ZHANG Chun-yang, WANG Yi-xian, RUAN Hang, KE Bo, LIN Hang. The strain characteristics and corresponding model of rock materials under uniaxial cyclic load/unload compression and their deformation and fatigue damage analysis [J]. Archive of Applied Mechanics, 2021, 91: 2481−2496.
[29] LIU Zhi-zhen, CAO Ping, LIN Hang, MENG Jing-jing, WANG Yi-xian. Three-dimensional upper bound limit analysis of underground cavities using nonlinear Baker failure criterion [J]. Transactions of Nonferrous Metals Society of China, 2020, 30: 1916−1927.
[30] ZHAO Yan-lin, ZHANG Lian-yang, LIAO Jian, WANG Wei-jun, LIU Qiang, TANG Li-ming. Experimental study of fracture toughness and subcritical crack growth of three rocks under different environments [J]. International Journal of Geomechanics, 2020, 20: 04020128.
[31] ZHANG Ke, LI Na, LIU Wen-lian, XIE Jian-bin. Experimental study of the mechanical, energy conversion and frictional heating characteristics of locking sections [J]. Engineering Fracture Mechanics, 2020, 228: 106905.
[32] LIN Hang, YANG Heng-tao, WANG Yi-xian, ZHAO Yan-lin, CAO Ri-hong. Determination of the stress field and crack initiation angle of an open flaw tip under uniaxial compression [J]. Theoretical and Applied Fracture Mechanics, 2019, 104: 102358.
[33] ZHOU Xiao-ping, WANG Yun-teng, ZHANG Jian-zhi, LIU Fei-nan. Fracturing behavior study of three-flawed specimens by uniaxial compression and 3D digital image correlation: sensitivity to brittleness [J]. Rock Mechanics and Rock Engineering, 2019, 52: 691−718.
[34] YANG Heng-tao, LIN Hang, CHEN Yi-fan, WANG Yi-xian, ZHAO Yan-lin, YONG Wei-xun, GAO Feng. Influence of wing crack propagation on the failure process and strength of fractured specimens [J]. Bulletin of Engineering Geology and the Environment, 2022, 81: 1−19.
[35] ZHAO Yan-lin, WANG Yi-xian, WANG Wei-jun, TANG Li-ming, LIU Qiang, CHENG Guo-ming. Modeling of rheological fracture behavior of rock cracks subjected to hydraulic pressure and far field stresses [J]. Theoretical and Applied Fracture Mechanics, 2019, 101: 59−66.
[36] WONG L N Y, EINSTEIN H H. Crack coalescence in molded gypsum and Carrara marble: Part 1. Macroscopic observations and interpretation [J]. Rock Mechanics and Rock Engineering, 2009, 42: 475−511.
[37] WONG L, LI Huan-qiang. Numerical study on coalescence of two pre-existing coplanar flaws in rock [J]. International Journal of Solids and Structures, 2013, 50: 3685−3706.
[38] ZHANG Xiao-ping, WONG L N Y. Crack initiation, propagation and coalescence in rock-like material containing two flaws: A numerical study based on bonded-particle model approach [J]. Rock Mechanics and Rock Engineering, 2013, 46: 1001−1021.
[39] YANG Sheng-qi. Crack coalescence behavior of brittle sandstone samples containing two coplanar fissures in the process of deformation failure [J]. Engineering Fracture Mechanics, 2011, 78: 3059−3081.
[40] CAO Ri-hong, CAO Ping, LIN Hang, MA Guo-wei, CHEN Yun. Failure characteristics of intermittent fissures under a compressive-shear test: Experimental and numerical analyses [J]. Theoretical and Applied Fracture Mechanics, 2018, 96: 740−757.
[41] LIN Qi-bin, CAO Ping, CAO Ri-hong, LIN Hang, MENG Jing-jing. Mechanical behavior around double circular openings in a jointed rock mass under uniaxial compression [J]. Archives of Civil and Mechanical Engineering, 2020, 20: 19.
[42] ZHAO Yan-lin, ZHANG Lian-yang, WANG Wei-jun, PU Cheng-zhi, WAN Wen, TANG Jing-zhou. Cracking and stress–strain behavior of rock-like material containing two flaws under uniaxial compression [J]. Rock Mechanics and Rock Engineering, 2016, 49: 2665−2687.
[43] HU Jian-hua, WEN Guan-ping, LIN Qi-bin, CAO Ping, LI Su. Mechanical properties and crack evolution of double-layer composite rock-like specimens with two parallel fissures under uniaxial compression [J]. Theoretical and Applied Fracture Mechanics, 2020, 108: 102610.
[44] LIN Qi-bin, CAO Ping, WEN Guan-ping, MENG Jing-jing, CAO Ri-hong, ZHAO Zhi-ye. Crack coalescence in rock-like specimens with two dissimilar layers and pre-existing double parallel joints under uniaxial compression [J]. International Journal of Rock Mechanics and Mining Sciences, 2021, 139: 104621.
[45] CHEN Yi-fan, LIN Hang, DING Xu-ran, XIE Shi-jie. Scale effect of shear mechanical properties of non-penetrating

horizontal rock-like joints [J]. Environmental Earth Sciences, 2021, 80: 1-10.

[46] TANG Yi, LIN Hang, WANG Yi-xian, ZHAO Yan-lin. Rock slope stability analysis considering the effect of locked section [J]. Bulletin of Engineering Geology and the Environment, 2021, 80: 7241−7251.

[47] ISRM. Suggested method for the complete stress-strain curve for intact rock in uniaxial compression [J]. International Journal of Rock Mechanics and Mining Sciences, 1999, 36: 279−289.

[48] ISRM. Suggested methods for determining the uniaxial compressive strength and deformability of rock materials [J]. International Journal of Rock Mechanics & Geomechanics Abstracts, 1979, 16: 138−140.

[49] PAN Bing, QIAN Ke-mao, XIE Hui-min, ASUNDI A. Two-dimensional digital image correlation for in-plane displacement and strain measurement: A review [J]. Measurement Science and Technology, 2009, 20: 062001.

单轴加载下含共面双节理双层复合类岩试样的力学行为与破坏特征

李 骋[1]，林 杭[1]，林奇斌[1]，汪亦显[2]，赵延林[3]，胡惠华[4]

1. 中南大学 资源与安全工程学院，长沙 410083；
2. 合肥工业大学 土木与水利工程学院，合肥 230009；
3. 湖南科技大学 资源环境与安全工程学院，湘潭 411201；
4. 湖南省交通规划勘察设计院有限公司，长沙 410219

摘 要：为研究节理与层理面对裂隙层状岩体裂纹演化的共同作用，对不同层理面倾角下，含多角度共面双节理的双层复合类岩试样进行单轴压缩试验和数字图像相关试验。由试验结果可知，层理面和节理对应力−应变曲线特征和强度参数有显著影响。试件的破坏模式分为 4 种不同类型。层理面的存在抑制了岩桥区域裂纹的贯通，层理面倾角的变化对裂纹扩展路径和破坏模式的转变有较大影响。对于层理面倾角为 30°和 45°的试件，节理倾角越大，层理面对试件破坏特征的影响越小。此外，观测到一种从层理面上萌生并且更容易在试件上层扩展的拉伸裂纹。

关键词：共面双节理；类岩试样；裂纹扩展；单轴加载；数字图像方法

(Edited by Xiang-qun LI)